Journal of Materials Chemistry C

Accepted Manuscript

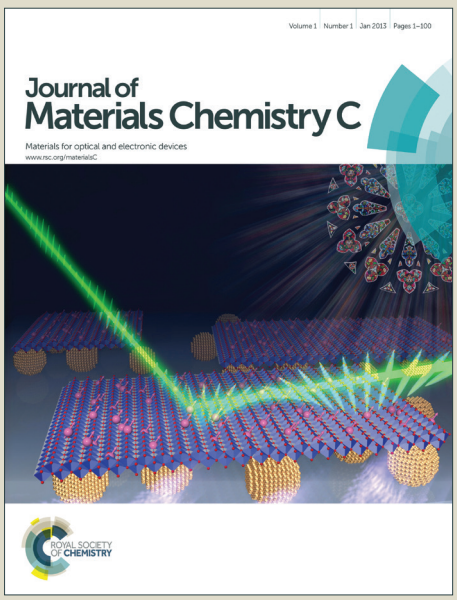

ROYAL SOCIETY OF CHEMISTRY

www.rsc.org/materialsC

Submitted to ***Journal of Materials Chemistry C***

Bio-Inspired Thermal-Responsive Inverse Opal Films with Dual Structural Colors based on Liquid Crystal Elastomer

Huihui Xing,[a,b] Jun Li,[a] Jinbao Guo*[a] and Jie Wei*[a,b]

[a] *College of Materials Science and Engineering, Beijing University of Chemical Technology, Beijing 100029, P. R. China.*

[b] *Beijing Engineering Research Center for the Synthesis and Applications of Waterborne Polymers, Beijing 100029, P. R. China.*

[*] *Correspondence to: guojb@mail.buct.edu.cn;*
weij@mail.buct.edu.cn.

Abstract: We develop a bio-inspired thermal-responsive micropatterned inverse opal film with dual structural colors based on liquid crystal elastomers (LCEs). Here inverse opal films are fabricated by infiltrating the LC precursor into the silica opal photonic crystal templates followed by UV irradiation, and then removing the silica spheres. Furthermore, the micropatterned inverse opal films with dual structural colors are fabricated by two-step photo-polymerization technique combining a DC electric field. The DC electric field is used to tune the lattice space of the silica opal templates at the second photo-polymerization stage. Additionally, the photonic band gaps of the LCE inverse opal films with dual structural colors can be reversibly switched by temperature because of the thermally induced molecular orientation change of the LCEs. This approach using to create bi-colored inverse opal with micropatterns opens up a new way to the development of the display and photonic applications.

1 Introduction

Photonic crystals (PCs) which have periodic structure with the periodicity at the scale of the wavelength of light exhibit photonic band gap (PBG) properties.[1-3] The propagation of certain wavelengths of light whose energy is in the band gap will be forbidden in the structure.[4, 5] Among this kind of materials, responsive PCs have attracted much attention due to their important applications in areas such as thermal and mechanical sensors,[6-11] biological and chemical sensors,[12-16] inks and paints,[17-19] and many optically active components.[20-22] Generally speaking, the stimulus have been proven to be any means that can effectively induce changes in the refractive indices,[14,23] the lattice constants,[24-27] and/or the degree of order in photonic structures.[28]

Liquid crystals (LCs) exhibit a large optical anisotropy due to their anisotropic molecular shape and alignment, and the refractive indices of LCs can be easily modulated by the change of temperature and/or the application of electric field. Based on these characteristics, thermal and/or electrical responsive opal or inverse opal PCs whose voids filled with LCs are fabricated.[29-31] In addition, photoresponsive PCs can be realized based on photochromic LCs.[32-35] In most cases, however, LCs are directly infiltrated into the voids of the PCs. As a result, the changes of the PBGs are limited due to that the modulation of PCs' PBGs derives from the change of the LCs' refractive indices.

LC elastomers (LCEs) are moderately cross-linked LC polymers which combine the elasticity properties of polymeric elastomers with the self-organization

characteristics of LCs.[36,37] As is well known, the most remarkable property of LCEs is the ability to change their shape reversibly after the application of certain external stimulus. LCEs are first introduced into PCs to act as inverse opal materials by Li *et al*. They developed a thermal-responsive inverse opal film using LCE together with a nematic LC (5CB).[38] By varying the temperature, the lattice constant together with the refractive indices changed and therefore the wavelength of the resultant Bragg peak could be tuned continuously. However, the reversibility of the Bragg peak shift is influenced by the 5CB molecules which are not linked to the LCEs by covalent bonds. Subsequently, they fabricated a new type of electrothermally driven inverse opal film based on cross-linked LCE without 5CB.[39] When the voltage is applied on the fabricated system, the heat produced by the graphite layer induces the deformation of the coated inverse opal film and thus the structural color is tuned. LCEs containing azobenzene groups have also been used to fabricate photo and thermal dual-responsive inverse opal materials.[28] However, only the reflectance intensities are modulated by light or temperature in this case.

In this study, we fabricate a kind of micropatterned inverse opal films with dual structural colors based on LCE by infiltrating the LC precursor into the three-dimentional silica opal PCs followed by UV irradiation, and then removing the silica opal templates. As is well known, dual structural colors or multiple structural colors are widespread phenomena in the biological world, which can be created by several different types of ordered structures on the same surfaces or by the different illumination angles from different parts in the same ordered nanostructure.[40] Inspired

by the dual structural colors of the butterflies and beetles, here a DC electric field is applied to tune the lattice space of the silica opal templates at the second photo-polymerization stage. After the etching process, a bi-colored inverse opal film with micropattern is achieved. Furthermore, a reversible thermal switching of these two PBGs of the micropatterned inverse opal films is investigated, and the relevant mechanisms are addressed in detail. This novel approach shows a great potential for fabrication of responsive PCs with dual/multiple structural colored complex patterns.

2 Experimental Section

2.1 Materials

All solvents and chemicals are of reagent quality and were used as received. The monoacrylate mesogenic monomer (A6OCB) was purchased from Bayi Space LCD. Tetraethyl orthosilicate (TEOS), ammonium hydroxide, anhydrous ethanol and photoinitiator Darocur 2959 were purchased from J&K Scientific Ltd. Nematic diacrylate monomer C6M was synthesized according to the method described by Broer *et al*.[41] Fig. 1a shows the chemical structures of A6OCB, C6M and Darocur 2959.

2.2 Preparation of LCE inverse opal films

Monodisperse silica spheres with sizes ranging from 200 to 330nm were produced by the Stőber method. A series of close-packed face-centred cubic (FCC) opal PCs were fabricated by a vertical deposition method in anhydrous ethanol with monodispersed silica spheres of different sizes. Fig. 1b outlines the preparation of the inverse opal films based on the LCEs. The LCE inverse opal films were prepared by

photo-polymerization method as follows. First, the monoacrylate mesogenic monomer A6OCB and nematic diacrylate monomer C6M with the molar ratio of 4:1 containing 0.1mol% of photoinitiator Darocur 2959 were dissolved in dichloromethane in order to mix well. C6M as a cross-linker in the LC system was also used to broaden the temperature range of the nematic phase because pure A6OCB exhibits the nematic phase within a narrow temperature range owing to the high crystallizability.[42] The silica opal PC was sandwiched in a glass cell with a 12μm cell gap setting by plastic spacers, and one of the glass plates was coated with rubbing-treated polyvinyl alcohol (PVA) alignment layer. After evaporation of the solvent, the LC monomers mixture was heated close to 85°C to keep the monomers in an isotropic phase and loaded into the cell by capillary action. Then the sample was cooled down to the nematic phase (60°C), and it was polymerized at 60°C under UV irradiation with the illumination intensity of 3mW/cm^2 for 10min. At last, LCE inverse opal film with bright structural color was obtained after silica opal template was etched by 2wt% HF.

2.3 Fabrication of patterned LCE inverse opal films

Patterned LCE inverse opal films with dual structural colors were fabricated by two-step photo-polymerization method. The electric field was applied to increase the lattice space of the silica opal PC templates at the second photo-polymerization stage. The silica opal PC, deposited on ITO glass plate, was sandwiched in an ITO glass cell with one ITO glass plate coated with rubbing-treated PVA alignment layer. Then the LC monomers mixture was filled in the cell. After that, the samples were locally irradiated by UV light through a photomask and the LC precursor in the

UV-irradiated regions polymerized.[43] Then a second UV exposure was carried out under a 55V electric field in order to increase the lattice space of silica opal PCs in the rest regions. Finally, a patterned LCE inverse opal film with dual structural colors was obtained after the silica particles were etched.

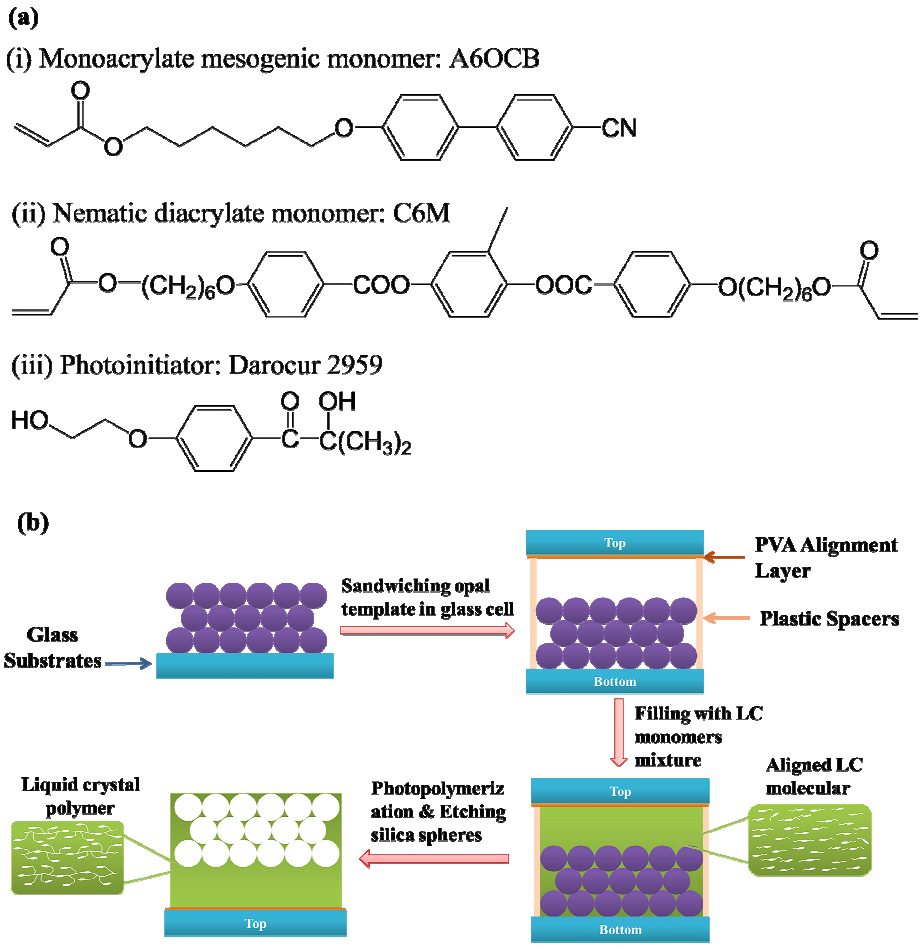

Fig. 1 (a) Chemical structures of A6OCB, C6M and Darocur 2959. (b) Schematic diagram illustrating the preparation of the LCE inverse opal films.

2.4 Measurements

The mesomorphic properties of the LC monomers mixture and the LCE inverse opal films were examined by polarizing optical microscope (POM, Leica, DM2500P) with a hot stage calibrated with an accuracy of ±0.1°C (Linkam, THMS-600).

Morphologies of silica opal PCs and inverse opal films were observed by scanning electron microscope (SEM, Hitachi S-4700). The thermodynamic properties were measured using differential scanning calorimeter (DSC, Pyris Diamond) with a heating and cooling rate of 10°C/min under a dry nitrogen purge. The reflection spectra were obtained by a fiber spectrometer (AvaSpec-2048) with a Y-type optical fiber in reflection mode, and the incident light and collect light were both vertical to the tested samples. The voltage was applied using a DC power supply (RXN-605D).

3 Results and Discussion

3.1 Inverse opal based on the LCEs

As shown in Fig. 1b, the inverse opal films are fabricated by infiltrating the LC precursor capable of UV photo-polymerization into the silica opal PCs, and then removing the silica opal templates. We firstly prepare a LC monomers mixture containing A6OCB and C6M with the molar ratio of 4:1, in which 0.1mol% of photoinitiator Darocur 2959 is added to induce UV photo-polymerization.

The thermodynamic properties and the phase transitions of the LC monomers mixture was investigated by POM. Fig. 2a is the POM image of LC monomers mixture before photo-polymerization; it clearly shows planar orientation of the LC molecules at 60°C of nematic phase. The LC monomers mixture was loaded into the cell by capillary action at 85°C, where the silica opal template was sandwiched and the LC monomers were in the isotropic phase. Then the sample was cooled down to 60°C, and polymerized at 60°C under UV irradiation. The LCE inverse opal film in nematic state was obtained after etching the silica spheres. As shown in Fig. 2b, the

LCE inverse opal film exhibits strong birefringence, which demonstrates that the nematic texture has been completely kept by the LCE inverse opal film. In addition, according to the DSC measurement results, the glass transition temperature (T_g) and the nematic–isotropic transition temperature (T_{NI}) of the LCE inverse opal film are around 41°C and 136°C, respectively.

The structure of the LCE inverse opal films were investigated by SEM. It should be noted that after etching the silica opal templates, the resulting LCE inverse opal films were directly used for SEM imaging. Fig. 2c-f show the SEM images of the opal structure composed of silica spheres with a diameter of 274nm and the LCE inverse opal film derived from the silica opal template. It can be seen that the silica opal template possesses a closely packed hexagonal structure (Fig. 2c), and the LCE inverse opal film has completely replicated the structure of the template (Fig. 2d). As can be seen from the cross-sectional SEM images in Fig. 2e and 2f, the LCE inverse opal film has a bilayer structure， and period ordered air holes embed in one side of the film. The thickness of the film is around 12μm and inverse opal part is less than 2μm, which are determined by the cell gap and the thickness of the silica opal template, respectively. It is worth noting the bilayer structure provides an enough space for the diffusions of the silica particles when an electric field is applied. Another important thing is that the residual LC layer is also beneficial to the switching of PBGs of inverse opal film as mentioned later. Fig. 2f is a higher magnification of the cross-sectional SEM image, it further demonstrates that the inverse opal film has a FCC crystal structure.

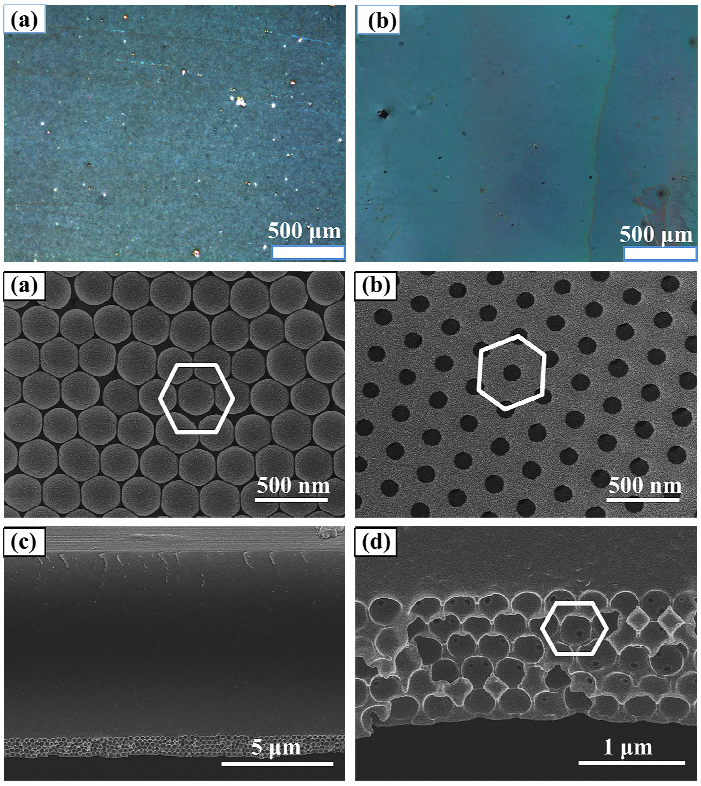

Fig. 2 (a) POM image of LC monomers mixture with the LC molecules planar aligned in the nematic state at 60°C. (b) POM image of the LCE inverse opal film. (c) SEM image of the silica opal template assembled of spheres with the diameter of 274nm. (d) SEM image of the LCE inverse opal film. (e) Cross-sectional SEM image of the LCE inverse opal film. (f) High magnification cross-sectional SEM image of the film.

3.2 Thermally induced PBG switching of the LCE inverse opal films

LCEs gain their actuation properties from the coupling of the elastomeric network and the LC units. As the phase transition to the isotropic state, the polymer chain changes into a spherical conformation, leading a reversible shape change.[37] Due to this interesting property of LCEs, the optical property of the inverse opal films based on LCEs can be reversibly switched. We investigated the reversible thermal-responsive behavior of LCE inverse opal films using fiber spectrometer in the reflection mode. Fig. 3a displays the reflection spectra for the LCE inverse opal films

as a function of temperature. When the LCE inverse opal film is heated from 30°C to 140°C, the reflection peak of the film has an obvious red-shift from 515nm to 565nm, leading the change of the structural color from blue-green to yellow-green. After the film is cooled down to 30°C, the PBG returns to its original wavelength as well as the structural color. This means that the thermal switching behavior of LCE inverse opal films is reversible. Fig. 3b illustrates the mechanism for the thermal-responsive behavior of the LCE inverse opal films. The shift of the PBG derives from the change of the molecule orientation and the following macroscopic deformation of both infiltrated LCEs and residual LCE sections. When the films are heated to make them close to their T_{NI}, the LC moieties become isotropic. They start to contract along the nematic director axis (parallel to the substrate) and expand in the other two directions. Thus, the d_{111} of the PC increases at the same time. As a result, the reflection peak shifts toward longer wavelength associated with a red-shift of the structural color, because the PBG of the LCE inverse opal film is directly proportional to the lattice constant.[44, 45] Since the LC moieties can return to original nematic state when the film is cooled down, the reflection peaks and structural colors of the films return to the original state.

3.3 Dual structural colored LCE inverse opal films

In order to get a dual structural colored inverse opal with micropattern, we firstly investigate the effect of the applied DC electric field on the PBG of the inverse opal film. We know that silica colloidal particles usually have negative surface electrical charge and show mobility in the presence of an electric field in the range of normal

pH.[46-48] So the electric field can be used to change the lattice spaces of silica opal templates and thus tune the PBGs of the inverse opal films.

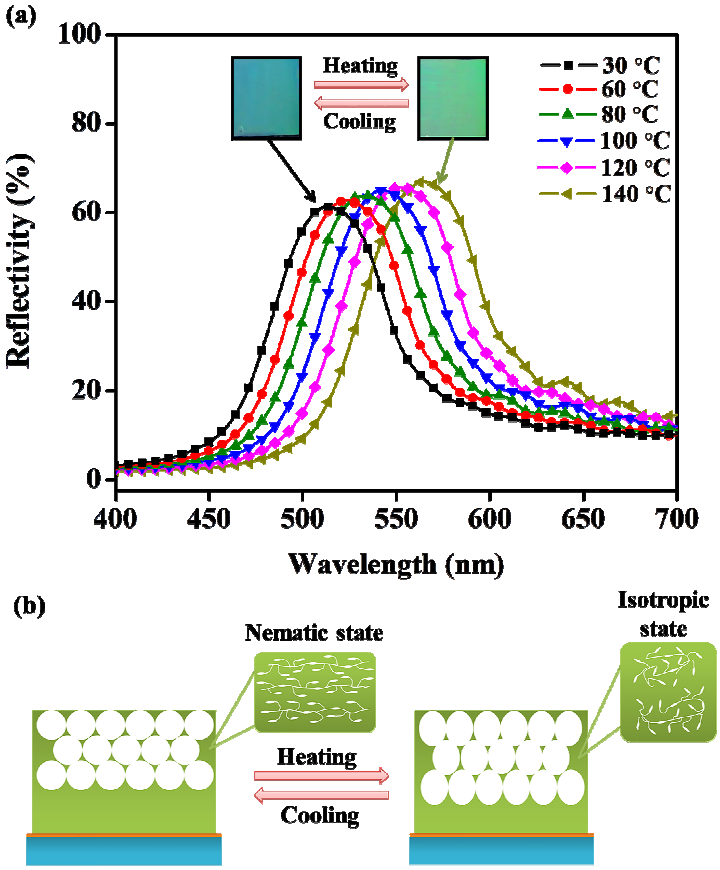

Fig. 3 (a) Reflection spectra reversible shifts and structural color reversible changes of the inverse opal film as a function of temperature. The size of the LCE inverse opal film in the image is about 12mm×10mm. (b) Schematic for the mechanism of the lattice space reversible change of LCE inverse opal films induced by temperature variation.

The cross-sectional SEM images of the LCE inverse opal films, fabricated without and with the application of electric field, are shown in Fig 4. By comparing the morphology in Fig. 4b with that in Fig. 4a, we find that the lattice space of the crystalline planes {111} (d_{111}) is increased for the LCE inverse opal film during the fabrication used an electric field. Meanwhile, the order degree of the air holes in the

film has a slight decrease. This is due to that the silica particles with a negative surface electrical charge move along the direction of the electric field in the ITO glass cell when an electric field is applied. Fig. 4c shows the reflection spectra for LCE inverse opal films fabricated without and with an electric field, respectively. The reflection peak of the LCE inverse film fabricated with the application of electric field has an obvious red-shift (about 100nm), and the film shows a bright orange-red structure color (Fig. 4c). It should be noted that the intensity of reflection peak of the film fabricated with an applied electric field is less than the one fabricated without the application of electric field. This may be due to the decrease of the order degree of the air holes in the LCE inverse opal film as mentioned in Fig. 4b.

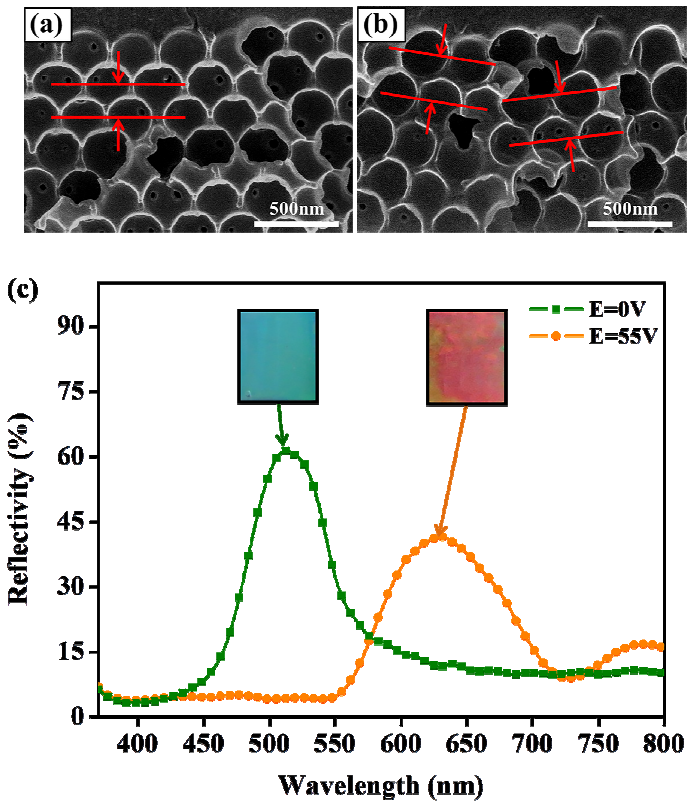

Fig. 4 Cross-sectional SEM images of LCE inverse opal films fabricated (a) without and (b) with the application of electric field. The width of the LCE inverse opal film

in the image is ca. 10mm. (c) Reflection spectra and structural colors for the LCE inverse opal films fabricated without and with the application of electric field.

Based on the modulation of the lattice space of the silica opal PCs by the electric field, micropatterned LCE inverse opal films with dual structural colors were fabricated by two-step photo-polymerization. Fig 5a illustrates the preparation of the strip patterned LCE inverse opal films. After the first local UV exposure through a photomask with strip pattern, the LC monomers are polymerized in the UV-irradiated regions and the closely packed hexagonal structure of silica opal PCs is frozen. Then the electric field is applied to increase the lattice space of the silica opal PCs in non-polymerized regions, and the increased lattice space is kept after a second UV exposure. The POM image of the patterned inverse opal film is shown in Fig. 5c. It can be seen that the patterned LCE film also exhibits strong birefringence, which is similar to that of the LC precursor (Fig. 5b). This suggests that the nematic state is kept in the patterned LCE films. In other words, the applied electric field in the second photopolymerization stage just induces an increasing of the silica template's lattice space in the non-polymerized regions, and does not change the LC molecular alignment. This result may have two explanations. First, the strength of applied electric field is not strong enough to induce the reorientation of LC molecular. Second, the anchoring strengths from the silica spheres and the PVA alignment layer are of benefit to the planar orientation of LC molecules.[31]

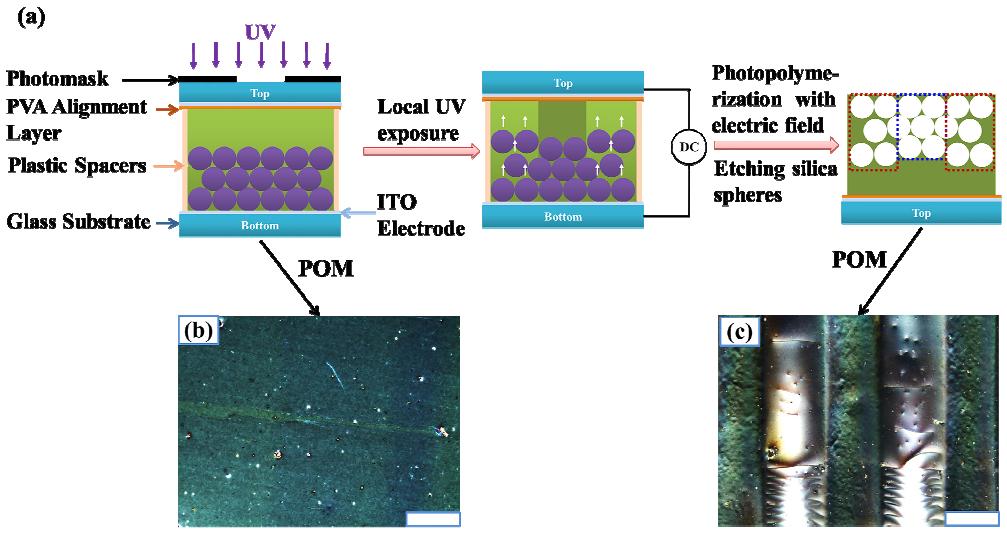

Fig. 5 (a) Schematic diagram illustrating the fabrication of the strip patterned LCE inverse opal films. (b) POM image of LC monomers mixture with the LC molecular planar aligned in the nematic state. (c) POM image of the strip patterned LCE inverse opal film. The scale bar in the image is 500μm.

Fig. 6a and b show the photograph of the strip patterned LCE inverse opal film and the corresponding schematic diagram of microscopic structure, respectively. It can be seen that the patterned LCE inverse opal film has bright green and orange-red strips with different lattice spaces. Correspondingly, the patterned LCE inverse opal films exhibited dual PBGs as shown in Fig. 6c. Furthermore, both the green and red PBGs can be reversibly tuned by temperature variation. As shown in Fig. 6c, when the films are heated, the green strips have a red-shift from 560nm to 604nm, and the orange-red strips also have a red-shift from 648nm to 696nm. As Fig. 5c indicates, the LC molecules in the green and orange-red strips are both at nematic state at room temperature. Therefore, the d_{111} of inverse opal structures in the green and orange-red strips both can be reversibly tuned by temperature. The tuning mechanism for the thermo-responsive behavior is the same as that for the inverse opal films with single

structural color mentioned above. The repeatability of PBGs' switch of the patterned LCE inverse opal film has been investigated. Fig. 7 shows five low-high temperature cycles of the strip patterned LCE inverse opal film. In each cycle, both the green and red strips' PBGs could shift from the original status to its maximum diffraction wavelength and then reversibly return back, which demonstrates that the film has a good stability. What's more, a reversible thermo-switching process of the patterned inverse opal sample on heating and cooling process has been demonstrated in a video file (see Supporting Information Movie 1).

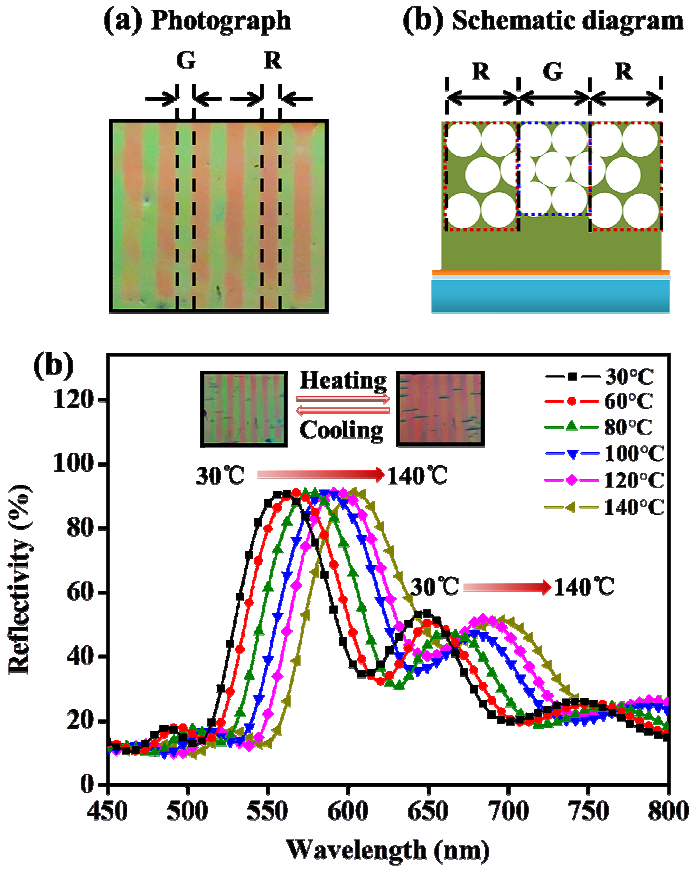

Fig. 6 (a) Photograph of the strip patterned LCE inverse opal film (the width is ca. 7mm) with bright green and red dual structure colors and (b) the corresponding schematic diagram of microscopic structure. (c) Reflection spectra reversible shifts and structural color reversible changes for the patterned films induced by temperature

variation. The size of the patterned LCE inverse opal film in the image is about 8mm×7mm.

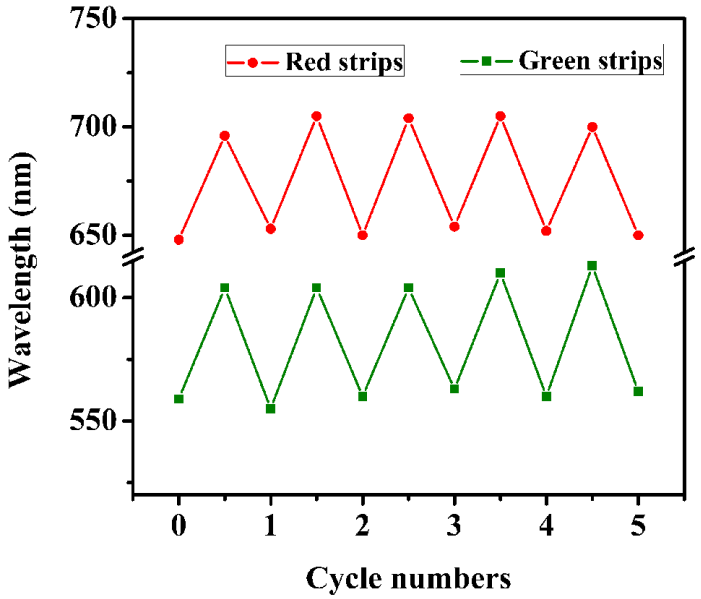

Fig. 7 Five low-high temperature cycles of the strip patterned LCE inverse opal film.

It should be noted that it is not difficult to achieve a complicated micropatterns on the LCE inverse opal film by changing the pattern design of the photomask. Red, green and blue structure colors in a single patterned film are also possible by optimizing the LC molecule and the size of the silica colloid particles. Here, controlling of the lattice spaces of silica opal template by electric field could ultimately lead to LCE-based inverse opal with different arrangement microdomains, allowing for the thermal switching of dual structural colors in inverse opal micropatterns. This facile control of inverse opal micropatterns' structural colors in the visible spectral ranges is of interest for displays, biomimetics and photonics applications.

4 Conclusions

In summary, a novel type of reversible thermo-responsive patterned inverse opal

films with dual structural colors are fabricated based on LCE. We demonstrate the formation of the micropatterned inverse opal film by two-step photo-polymerization technique combining a DC electric field to tune the lattice space of the silica opal templates. The results demonstrate that the dual PBGs of the patterned LCE inverse opal films can be reversibly switched by temperature, in which both of these two PBGs have around 50nm red-shift. This is mainly because of the thermally induced the change of molecular orientation and the following macroscopic deformation of LCE. These dual structural colored and thermo-responsive LCE inverse opal films are of interest for a variety of applications varying from color displays to optical actuators and sensors.

Acknowledgements

The authors are grateful for the financial support by the National Natural Science Foundation (Grant No. 51373013 and 51173013) and Beijing Young Talents Plan (YETP0489).

References

1. G. von Freymann, V. Kitaev, B. V. Lotsch and G. A. Ozin, *Chem. Soc. Rev.*, 2013, **42**, 2528.

2. C. López, *Adv. Mater.*, 2003, **15**, 1679.

3. M. Salaün, B. Corbett, S. B. Newcomb and M. E. Pemble, *J. Mater. Chem.*, 2010, **20**, 7870.

4. A. Stein, B. E. Wilson and S. G. Rudisill, *Chem. Soc. Rev.*, 2013, **42**, 2763.

5. P. Viktorovitch, E. Drouard, M. Garrigues, J. L. Leclercq, X. Letartre, P. R. Romeo and C. Seassal, *C. R. Physique*, 2007, **8**, 253.

6. T. S. Deng, J. Y. Zhang, K. T. Zhu, Q. F. Zhang and J. L. Wu, *Opt. Mater.*, 2010, **32**, 946.

7. T. S. Deng, J. Y. Zhang, K. T. Zhu, Q. F. Zhang and J. L. Wu, *Mater. Chem. Phys.*, 2011, **129**, 540.

8. K. Matsubara, M. Watanabe and Y. Takeoka, *Angew. Chem. Int. Edit.*, 2007, **46**, 1688.

9. Y. Takeoka and M. Watanabe, *Langmuir*, 2003, **19**, 9104.

10. E. P. Chan, J. J. Walish, A. M. Urbas and E. L. Thomas, *Adv. Mater.*, 2013, **25**, 3934.

11. L. Duan, B. You, L. Wu and M. Chen, *J. Colloid Interface Sci.*, 2011, **353**, 163.

12. W. Hong, X. Hu, B. Zhao, F. Zhang and D. Zhang, *Adv. Mater.*, 2010, **22**, 5043.

13. Z. H. Wang, J. H. Zhang, J. Xie, C. A. Li, Y. F. Li, S. Liang, Z. C. Tian, T. Q. Wang, H. Zhang, H. B. Li, W. Q. Xu and B. Yang, *Adv. Funct. Mater.*, 2010, **20**,

3784.

14. C. Liu, G. Gao, Y. Zhang, L. Wang, J. Wang and Y. Song, *Macromol. Rapid Commun.*, 2012, **33**, 380.

15. N. Griffete, H. Frederich, A. Maitre, S. Ravaine, M. M. Chehimi and C. Mangeney, *Langmuir*, 2012, **28**, 1005.

16. P. Yan, G. T. Fei, G. L. Shang, B. Wu and L. D. Zhang, *J. Mater. Chem. C*, 2013, **1**, 1659.

17. J. X. Wang, L. B. Wang, Y. L. Song and L. Jiang, *J. Mater. Chem. C*, 2013, **1**, 6048.

18. R. Xuan and J. Ge, *Langmuir*, 2011, **27**, 5694.

19. J. Ge, Y. Hu and Y. Yin, *Angew. Chem. Int. Edit.*, 2007, **46**, 7428.

20. K. Hwang, D. Kwak, C. Kang, D. Kim, Y. Ahn and Y. Kang, *Angew. Chem. Int. Edit.*, 2011, **50**, 6311.

21. A. C. Arsenault, D. P. Puzzo, I. Manners and G. A. Ozin, *Nat. Photonics*, 2007, **1**, 468.

22. J. Ge and Y. Yin, *Angew. Chem. Int. Edit.*, 2011, **50**, 1492.

23. H. Li, L. Chang, J. Wang, L. Yang and Y. Song, *J. Mater. Chem.*, 2008, **18**, 5098.

24. P. Kang, S. O. Ogunbo and D. Erickson, *Langmuir*, 2011, **27**, 9676.

25. Q. B. Zhao, A. Haines, D. Snoswell, C. Keplinger, R. Kaltseis, S. Bauer, I. Graz, R. Denk, P. Spahn, G. Hellmann and J. J. Baumberg, *Appl. Phys. Lett.*, 2012, **100**, 101902-1.

26. H. Hu, Q. W. Chen, K. Cheng and J. Tang, *J. Mater. Chem.*, 2012, **22**, 1021.

27. T. Ito, C. Katsura, H. Sugimoto, E. Nakanishi and K. Inomata, *Langmuir*, 2013, **29**, 13951.

28. J. Q. Zhao, Y. Y. Liu and Y. L. Yu, *J. Mater. Chem. C*, 2014, **2**, 10262.

29. M. Ozaki, Y. Shimoda, M. Kasano and K. Yoshino, *Adv. Mater.*, 2002, **14**, 514.

30. L. Criante and F. Scotognella, *J. Phys. Chem. C*, 2012, **116**, 21572.

31. Y. Shimoda, M. Ozaki and K. Yoshino, *Appl. Phys. Lett.*, 2001, **79**, 3627.

32. Y. J. Liu, Z. Y. Cai, E. S. P. Leong, X. S. Zhao and J. H. Teng, *J. Mater. Chem.*, 2012, **22**, 7609.

33. S. Kubo, Z.-Z. Gu, K. Takahashi, A. Fujishima, H. Segawa and O. Sato, *Chem. Mater.*, 2005, **17**, 2298.

34. S. Kubo, Z. Z. Gu, K. Takahashi, A. Fujishima, H. Segawa and O. Sato, *J. Am. Chem. Soc.*, 2004, **126**, 8314.

35. M. Moritsugu, T. Shirota, S. Kubo, T. Ogata, O. Sato and S. Kurihara, *J. Polym. Sci. Pol. Phys.*, 2009, **47**, 1981.

36. D. Iqbal and M. H. Samiullah, *Materials*, 2013, **6**, 116.

37. C. Ohm, M. Brehmer and R. Zentel, *Liquid Crystal Elastomers: Materials and Applications*, Springer-Verlag Berlin, Berlin, 2012, **250**, 49.

38. G. Wu, Y. Jiang, D. Xu, H. Tang, X. Liang and G. Li, *Langmuir*, 2011, **27**, 1505.

39. Y. Jiang, D. Xu, X. S. Li, C. X. Lin, W. N. Li, Q. An, C. A. Tao, H. Tang and G. T. Li, *J. Mater. Chem.*, 2012, **22**, 11943.

40. Y. Y. Diao, X. Y. Liu, G. W. Toh, L. Shi and J. Zi, *Adv. Funct. Mater.*, 2013, **23**, 5373.

41. D. J. Broer, J. Boven, G. N. Mol and G. Challa, *Makromo. Chem.*, 1989, **190**, 2255.

42. Y. Sawa, K. Urayama, T. Takigawa, A. DeSimone and L. Teresi, *Macromolecules*, 2010, **43**, 4362.

43. T. Zhang, Q. W. Dong, W. Zhang and J. Wei, *Chin. J. Polym. Sci.*, 2013, **31**, 444.

44. S. H. Park and Y. Xia, *Langmuir*, 1999, **15**, 266.

45. I. I. Tarhan and G. H. Watson, *Phys. Rev. B Condens. Matter*, 1996, **54**, 7593.

46. M. Trau, D. A. Saville and I. A. Aksay, *Science*, 1996, **272**, 706.

47. J. Kim and D. F. Lawler, *Bull. Korean Chem. Soc.*, 2005, **27**, 1083

48. Y. J. Huang, C. H. Lai and P. W. Wu, *Electrochem. Solid-State Lett.*, 2008, **11**, P20.

Table of contents entry

Text:

The fabrication of inverse opal micropatterns based on liquid crystal elastomers with dual structure colors and their thermal switching behaviors are described.

Color graphic: